



Bioinspired sutured materials for strength and toughness: Pullout mechanisms and geometric enrichments

Idris A. Malik, Francois Barthelet*

Department of Mechanical Engineering, McGill University, 817 Sherbrooke Street West, Montreal, QC H3A 2K6, Canada



ARTICLE INFO

Article history:

Received 9 October 2017

Revised 24 December 2017

Available online 6 January 2018

Keywords:

Sutured lines

Shape descriptors

Analytical models

Finite element models

Optimization

ABSTRACT

Hard structural elements in nature are often joined with sutures lines, as seen in human skull, cephalopods or turtle shell. These sutures can arrest cracks, and can provide flexibility for respiration, locomotion or growth. In this paper we introduce a morphometric method to capture the complex shape of sutured interfaces using only a few parameters. The method is simple, and can capture relatively complex suture geometries with re-entrants, interlocking features. The study starts with a simple jigsaw-like model which is enriched with additional features (plateau regions in dovetail-like sutures, multiple locking sites). For each case, closed form and finite elements solutions are developed to capture the full non-linear pullout response and to predict the maximum stress (and potential fracture) in the solid material. These models were then used to identify the geometries and interface properties (friction) that lead to optimum combinations of strength and energy absorption. Suture designs that reduced frictional stress with low coefficient of friction or with multiple contact points were the most efficient. The results can serve as guidelines to design and optimization of non-adhesive sutures with arbitrary shapes made of arc of circles and lines. We found that the best designs involve low coefficient of friction, which raises an interesting hypothesis on the function of the protein layer in natural sutured lines: This soft layer could act as “lubricant” to prevent the fracture of the solid structures.

© 2018 Elsevier Ltd. All rights reserved.

1. Introduction

Components made of hard materials can be joined by suture lines, a structural feature found in multiple examples in nature: shells of cephalopods (Allen, 2007), human skull (Coats and Margulies, 2006; Maloul et al., 2014; Miura et al., 2009), carapace of turtle (Achrai et al., 2014; Chen et al., 2015; Zhang et al., 2012), wood peckers beak (Lee et al., 2014) (Fig. 1), and in many other hard biological materials where weak interfaces govern deformation and fracture mechanisms (Dunlop et al., 2011; Barthelet et al., 2016). In these examples, stiff skeletal material (mineralized proteinaceous matrices, keratin) are joined by thin lines of interfacial material which are much softer. The geometrical complexity of the suture lines ranges from nearly straight sutured interfaces in new born baby skull (Coats and Margulies, 2006; Miura et al., 2009), to more complex ceratitic and ammonitic sutures with fractals geometries (Allen, 2007; Li et al., 2012; Lin et al., 2014). In cephalopods such as ammonoid, which produce angular or dendritic sutures, the complexity of the suture lines varies across species (Allen, 2007), or with growth as seen in the inter-

digitating suture lines in human skull which become more complicated from infant to adult (Miura et al., 2009; Maloul et al.,). Some of these interfaces form anti-trapezoidal sutures which are interlocked as seen in linking the girdles of diatoms (Genkal and Popovskaya, 2008; Manoylov et al., 2009), while others display sinusoidal interfaces which increases resistance to crack propagation (Li et al., 2011).

The softer interface materials at the sutures enable the relative displacement and/or relative rotation of harder structural components, which facilitates locomotion, respiration or growth (Lin et al., 2014; Li et al., 2011). Sutured interfaces can also absorb impact energy (Lee et al., 2014), channel the propagation of cracks into toughening configurations, or act as a source of local deformation that can spread energy dissipative mechanisms throughout large volumes (Barthelet et al., 2007; Fratzl et al., 2004). The geometry of sutured lines largely governs their mechanical response (Li et al., 2012, 2013; Lin et al., 2014, 2014; Zavattieri et al., 2008). In particular, interlocking geometrical features can increase strength and energy dissipation (Malik and Barthelet, 2016; Mirkhalaf et al., 2014; Mirkhalaf and Barthelet, 2017; Haldar et al., 2017). We recently developed analytical and finite element models that capture the complete nonlinear pullout response of sutures with simple interlocking jigsaw-like geometries, based on frictional contact and linear elasticity (Malik et al., 2017). These models demon-

* Corresponding author.

E-mail address: francois.barthelet@mcgill.ca (F. Barthelet).

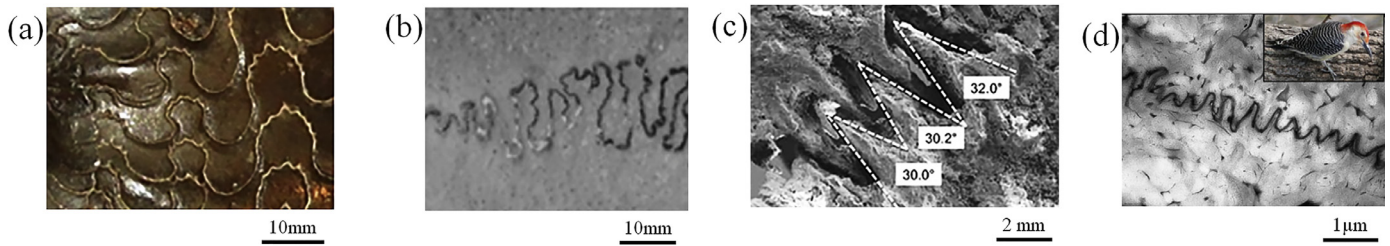


Fig. 1. Examples of sutured interfaces in nature: (a) Ammonite shell (*Ceratitic ammonoid*) with intricate suture lines (Lin et al., 2014), (b) Pan troglodytes cranial sutures (adapted from Cray et al., 2010), (c) Osteoderms of a leatherback sea turtle shell (adapted from Chen et al., 2015), (d) red-bellied woodpecker (*Melanerpes carolinus*) beak (adapted from Lee et al., 2014).

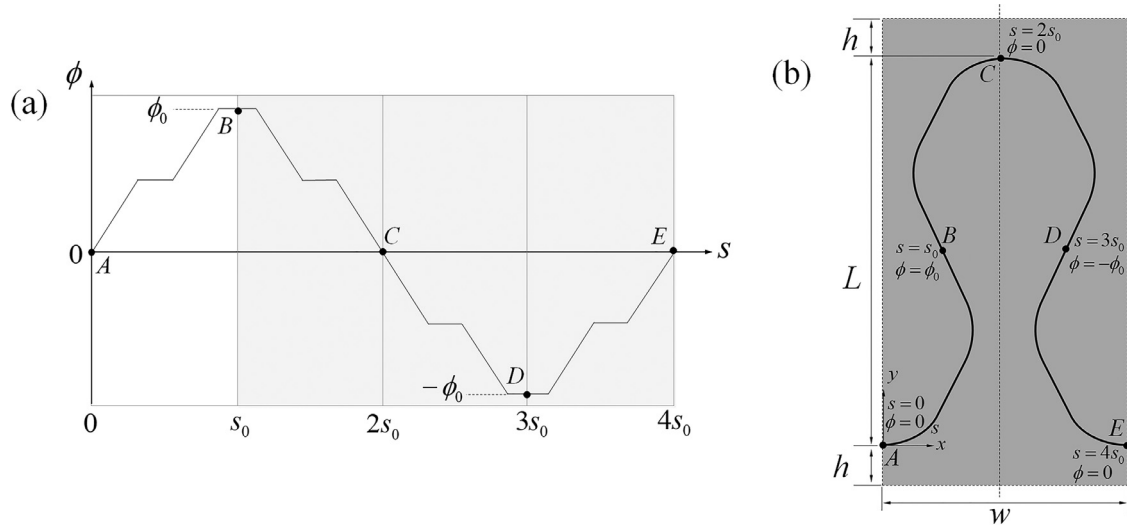


Fig. 2. (a) A parametric (ϕ - s) curve showing the cumulative angular function as function of curvilinear position; (b) Suture profile in (x,y) reconstructed from the (ϕ - s) function.

strated how geometry and local friction coefficient govern stiffness, strength and energy absorption, and how geometry and friction can be tuned to optimize the mechanical response. In this article we present new extensions to these models, where we consider sutures with more complex morphologies: dovetail-like sutures and sutures with two or more pairs of locking sites. For each type of suture we performed an exhaustive search to determine the design parameters which maximize strength and energy absorption. A comparative study of the different suture morphologies is provided at the end of the discussion.

2. Overview of the suture geometry

Capturing the two-dimensional geometry of a curved suture line requires robust, high fidelity yet relatively simple mathematical models. Methods used in the past include descriptive methods, pattern-matching using geographic information systems, complexity indices, and morphometric methods (Allen, 2007; Manoylov et al., 2009; Saunders et al., 1999). In this work, we used a simple 2D shape descriptor approach similar to the morphometric method. Shape descriptors are mathematical objects which can capture geometrical features in a simplified and condensed fashion, for example the radius of a circle, the surface of an area, or geometrical eccentricity (Fang et al., 2015; Kim and Kim, 2000). The shape descriptor we used in this study is based on a cumulative angular function of the contour of the suture ϕ as function of the curvilinear position s along the contour (Fig. 2). The approach is versatile and more importantly, it enables the modelling of suture lines with re-entrant, interlocking features. For this study we

only considered $\phi(s)$ functions that are multilinear (Fig. 2a). The 2D profile of the suture can be reconstructed from the $\phi(s)$ function in the x - y coordinate system using:

$$\begin{cases} x(s) = \int_0^s \cos(\phi(s)) ds \\ y(s) = \int_0^s \sin(\phi(s)) ds \end{cases} \quad (1)$$

Where the point $x=0$ and $y=0$ coincides with $s=0$. This process generates a periodic unit cell of the suture (Fig. 2b).

For this study we required the contour (x - y) of the suture to be periodic and continuous. We also required contours with no sharp corner or kinks which would generate stress concentrations and lead to sub-optimal designs. The function $\phi(s)$ therefore had to be continuous. In addition, for a suture line whose general orientation is aligned with the axis x , the local tangential angle ϕ must take a zero value at least once within the periodic unit cell. For simplicity we chose $\phi(0)=0$. In this work we also only considered sutures with a symmetry about line $x=w/2$, where w is the width of the unit cell in the x - y space. This symmetry implies that the function $\phi(s)$ is antisymmetric about the line $s=2s_0$ (Fig. 2a). Finally, we sought optimum geometries for the suture and therefore we focused on geometries that produces identical stresses on either side of the suture line, because asymmetric sutures lines would be sub-optimal with one side inevitably be “better” than the other. Therefore we only considered suture lines with a 180° rotational symmetry, which implies that the function $\phi(s)$ is symmetric about the line $s=s_0$ (Fig. 2a). Considering these symmetries, the functions $\phi(s)$ only need to be defined over a quarter of the curvilinear

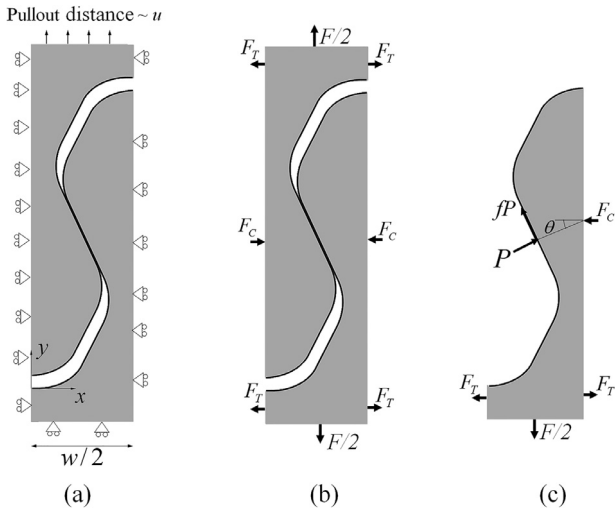


Fig. 3. (a) Half-unit cell for the suture with symmetry and boundary conditions applied. (b) Free body diagram of the half-unit cell; (c) free body diagram of the lower tab only, exposing the normal and frictional forces transmitted at the contact between the tabs.

length of the contour in the periodic cell ($0 \leq s \leq s_0$, Fig. 2). The first quarter of the $(x-y)$ contour was reconstructed using Eq. (1) up to $s = s_0$, and a 180° rotational symmetry was then applied about points $x(s_0), y(s_0)$, in order to produce a half unit cell which was used for the analysis of kinematics, forces and stresses. For display purposes, the full unit cell may be reconstructed with a simple symmetry (Fig. 2b). The full unit cell has width w , and height $L + 2h$ where L is the projected length of the suture on the y axis, and h is the height of two regions included in the model on either sides of the suture. The width, w and the height, L of the suture

are given by:

$$\begin{cases} w = 2 \int_{s=0}^{2s_0} \cos(\phi(s)) ds \\ L = \int_{s=0}^{2s_0} \sin(\phi(s)) ds \end{cases} \quad (2)$$

This “shape generating algorithm” has a few properties that are useful to outline here. The local radius of curvature R on the $(x-y)$ profile of the suture is related to the local suture angle by $Rd\phi = ds$, so that the local slope of $\phi(s)$ is:

$$\frac{d\phi}{ds} = \frac{1}{R} \quad (3)$$

An important implication is that horizontal segments in the $\phi(s)$ function ($\phi'(s)=0$) correspond to straight segments on the $(x-y)$ profile ($R = \infty$). This shape descriptor approach was used to generate a wide array of suture geometries, and the pullout mechanics of each of these geometries was captured with the model described below.

3. Pullout models

In terms of mechanics, this study focused on the full pullout response of the suture along the y direction (Fig. 3). We only considered sutures with no adhesive at the interfaces, so that the pullout response was governed only by contact mechanics, friction and geometric interlocking. The solid part of the suture was assumed to be isotropic and linear elastic (modulus E and Poisson’s ratio ν), and 2D plane stress conditions were used. Fig. 3a shows a representative volume element (RVE) of the suture geometry. The pullout was simulated using a displacement controlled boundary conditions:

$$\begin{cases} u_y(x, -h) = 0 \\ u_y(x, L+h) = u \end{cases} \quad (4)$$

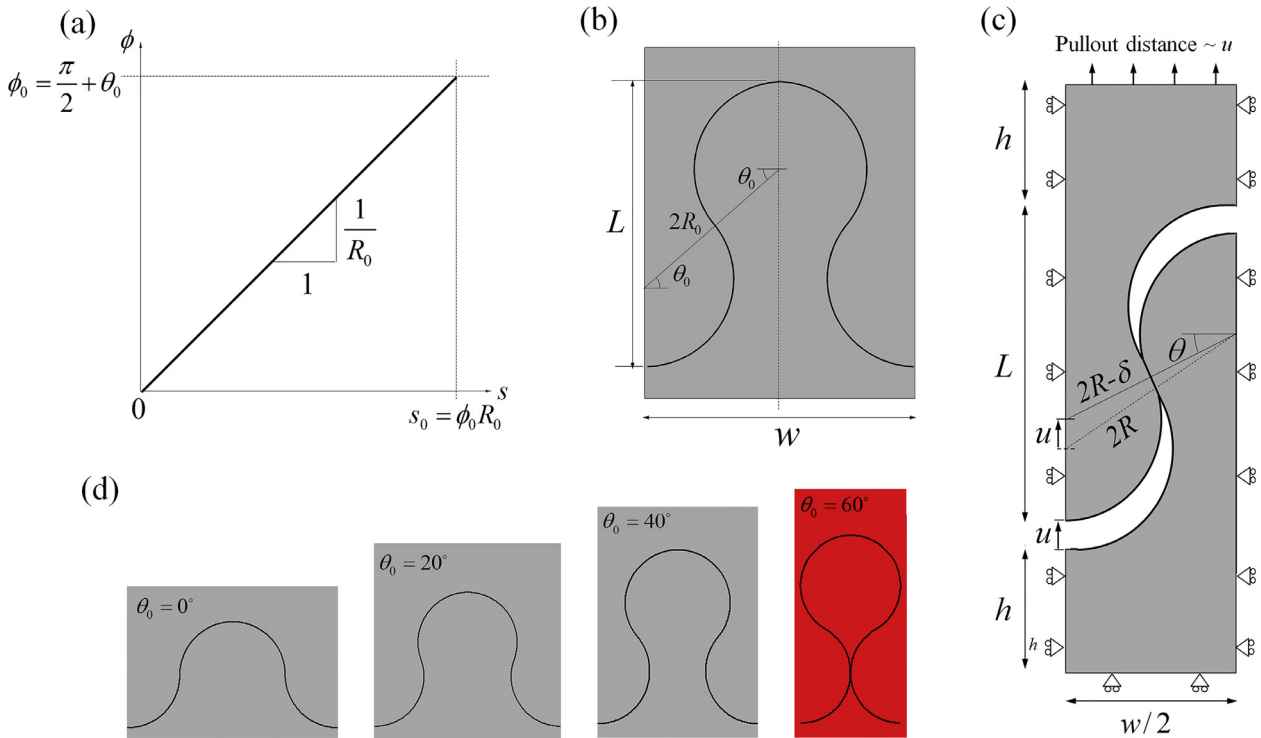


Fig. 4. (a) $(\phi-s)$ curve for a one-parameter suture; (b) Corresponding profile; (c) model with symmetry and boundary conditions; (d) The “strength” of the geometrical interlocking is governed by the interlocking angle θ_0 , where $\theta_0 < 60^\circ$ to prevent the re-entrant regions of the tabs to intersect (case highlighted in red). (For interpretation of the references to colour in this figure legend, the reader is referred to the web version of this article.)

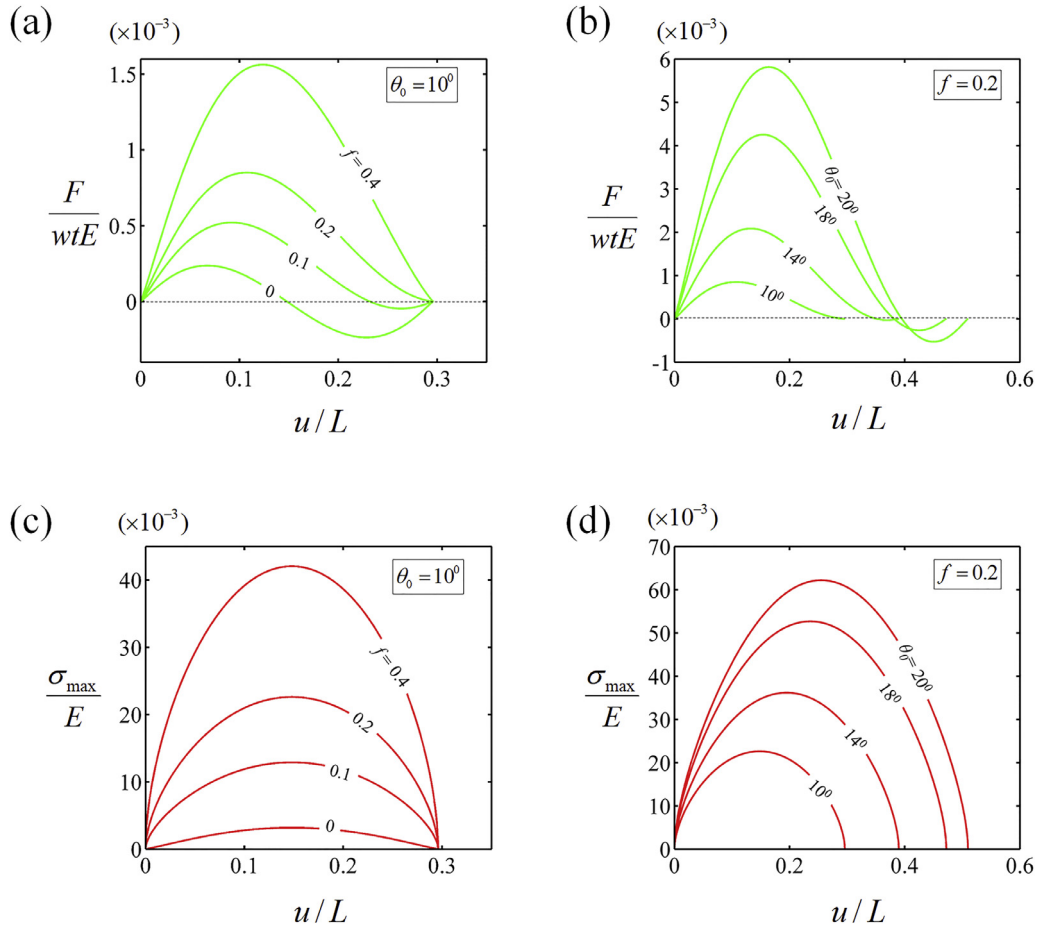


Fig. 5. Effects of (a) friction f and (b) interlocking angle θ_0 on the pullout response of the suture; effects of (c) friction f and (d) interlocking angle θ_0 on maximum tensile stress in the solid tabs.

Where h is the height of the upper and lower portion from the suture interface (Fig. 2c). The sides of the model were subjected to the periodic boundary conditions:

$$\begin{cases} u_x(w/2, y) - u_x(-w/2, y) = w\bar{\epsilon}_x \\ u_y(w/2, y) = u_y(-w/2, y) \end{cases} \quad (5)$$

Where $\bar{\epsilon}_x$ is the average strain in the x (transverse) direction. The geometry and loading conditions are symmetric about the y -axis so that:

$$u_x(x, y) = -u_x(-x, y) \quad (6)$$

Combining Eqs. (5) and (6), the periodic boundary conditions are written:

$$\begin{cases} u_x(0, y) = 0 \\ u_x(w/2, y) = \frac{w}{2}\bar{\epsilon}_x \end{cases} \quad (7)$$

In cases where h is sufficiently large, the stiffness of the solid regions in the transverse direction is high enough to neglect any deformation in the transverse direction, i.e. $\bar{\epsilon}_x = 0$. Equations (7) then become (Fig. 3a):

$$\begin{cases} u_x(0, y) = 0 \\ u_x(w/2, y) = 0 \end{cases} \quad (8)$$

When the upper suture is pulled along the y axis, the interlocking at the suture generates a pullout force F along the y axis ($F/2$ on the half unit cell, Fig. 3b). The contact forces at the interfaces also generate a horizontal component, giving rise to a compressive forces F_c along the x axis. Because the net horizontal force on the

unit cell is zero, the compressive forces in the suture region must be balanced by tensile forces F_T transmitted on either sides of the suture line (Fig. 3b). Fig. 3c shows a free body diagram of the lower section of the suture, which exposes the contact forces transmitted at the interfaces. These forces can be decomposed into normal force(s) P_i and frictional force(s) fP_i (only one contact force is showed on Fig. 3c, but there might be more sets of contact forces depending on the design of the suture). These contact forces will translate into a pullout force through the equation:

$$F = 2 \sum_{i=1}^N P_i (\sin \theta + f \cos \theta) \quad (9)$$

The set of forces shown in Fig. 3 also generate stresses in the solid parts of the suture which must be monitored because fracturing the material would abort the pullout mechanisms and cancel their potential benefits. Experiments and stress analysis have shown that for brittle material in sliding dry contact, the highest tensile stresses occur at the surface of the suture, at the edge of the contact area (Malik et al., 2017). For each of the geometries presented below, the maximum tensile stress in the solid part was calculated for the entire pullout sequence.

We also used numerical methods for the models, with a combination of finite element simulations (ANSYS parametric design language) interfaced with Matlab (R2016a, MA, US). $\phi(s)$ curves were generated and automatically transformed into suture geometries into x - y profiles using a Matlab. The same code was used to automatically generate APDL input files for ANSYS. The models were meshed with quadratic, plane stress element (PLANE 183),

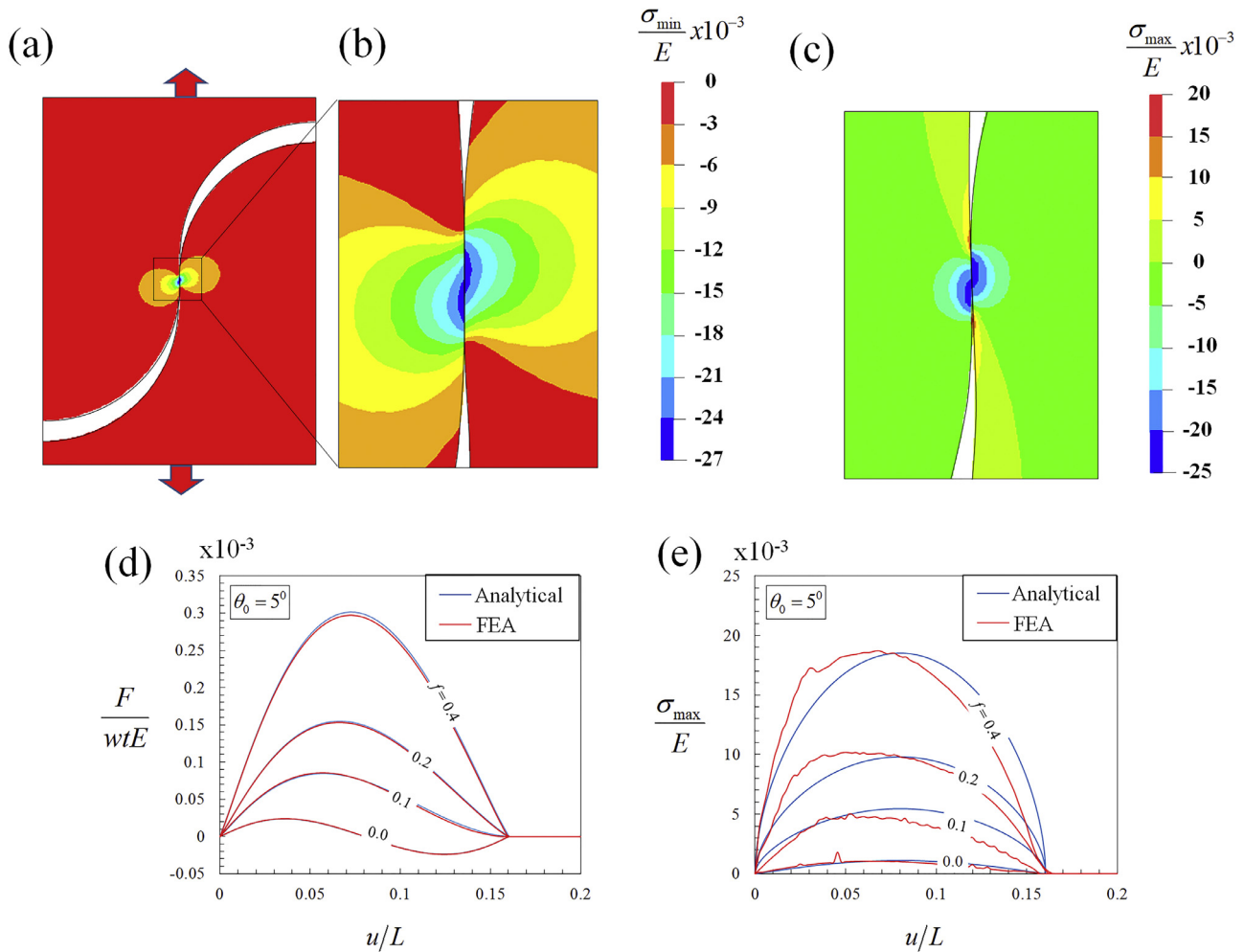


Fig. 6. (a) and (b) contour plots of maximum pressure (minimum principal stress) for $\theta_0 = 5^\circ$ and $f = 0.4$; (c) contour plot of maximum principal stress (maximum tensile stress in the tabs); (d) and (e) traction and maximum tensile stresses as function of pullout distance showing a good agreement between the analytical and finite elements results (extracted from Malik et al., 2017).

and contact elements (CONTA 172, TARGE 169, symmetric contact) were used to simulate sliding and frictional contact at the interface. To appropriately mesh the model we used an adaptive meshing approach for each geometry. A first model was run with a uniform mesh, and the mesh was automatically refined at the regions of highest stresses. The procedure was repeated automatically until the results for pullout response and maximum tensile stress in the solid converged, ensuring mesh independent results. Typically the size of the elements in the converged mesh was about $R/5000$ in the contact region, where R is the radius of curvature. The number of time steps in simulation was also adapted automatically to ensure converged results, typically about 500. The results were automatically post-processed using ANSYS ADPL and Matlab. This fully automated exploration procedure enabled the evaluation of thousands of models with different suture geometries and coefficients of friction.

4. Exploration of suture geometries

In this section we explore the effect of several suture geometries on pullout behavior. We organized the exploration by starting with a simple design (single jigsaw sutures) based on a single geometrical parameter. We then progressively enriched the geometry of the suture by adding more geometrical features through additional parameters: dovetail-like sutures, double locking sutures, N-

locking sutures. Within each type of geometry we sought the geometrical parameters and materials properties that lead to optimum combinations of high strength and high energy absorption, while preventing the brittle fracture of the solid part of the suture.

4.1. Single jigsaw sutures

The single jigsaw sutures are the simplest form of geometric parameters, with a radius of curvature R_0 , and a locking angle θ_0 ([27], Fig. 4). Since the mechanisms captured here have no specific length scale, all results are normalized by the size of the model, leaving θ_0 the only geometrical parameter. The other geometric parameters can be found using Eqs. (2) and (4):

$$\begin{cases} \phi_0 = \theta_0 + \pi/2 \\ w = 4R_0 \sin \phi_0 \\ L = 2R_0(1 - \cos \phi_0) \end{cases} \quad (10)$$

The length of the 1/4 contour of the suture is $s_0 = R_0\phi_0$ and the $\phi(s)$ function is simply (Fig. 4a):

$$\phi(s) = \frac{s}{R_0}, 0 \leq s \leq s_0$$

Fig. 4b shows the reconstructed profile of the suture, which consists of four appended arcs of circle. The level of interlocking

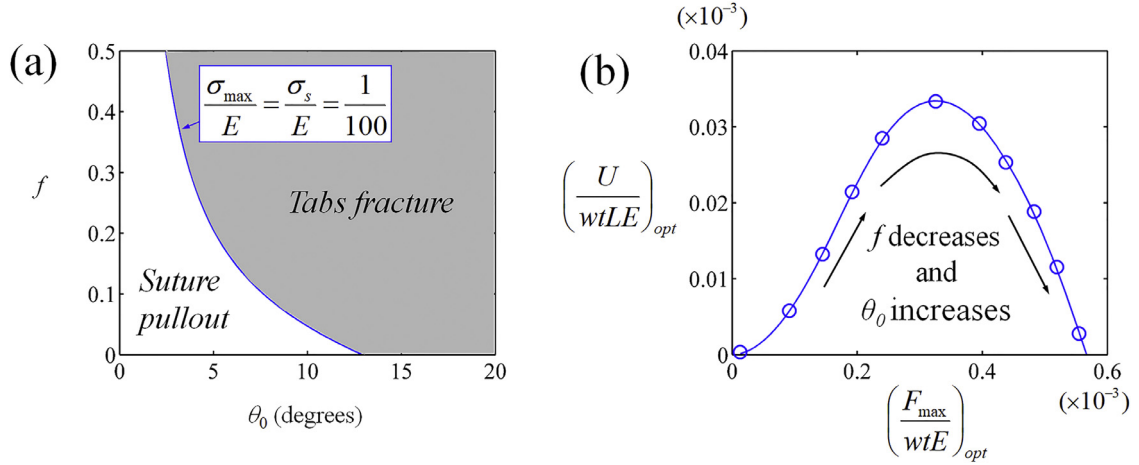


Fig. 7. (a) Possible combinations of the parameters θ_0 and f for optimum designs; (b) Optimum energy absorbed and optimum pullout strength calculated using the constraint $\sigma_s/E=1/100$.

increases when θ_0 increases as shown on Fig. 4d, up to the extreme case $\theta_0=60^\circ$ where the suture line intersects which corresponds to the maximum geometrically allowed locking angle. Sutures with $\theta_0 \geq 60^\circ$ were therefore excluded from the exploration as physically unacceptable. An analytical solution for the pullout response based on simple kinematics and contact mechanics was presented in a previous article (Malik et al., 2017), with the main results are summarized below. Fig. 4b and c give the kinematics relations (Malik et al., 2017):

$$(2R_0 - \delta) \cos \theta = 2R_0 \cos \theta \tag{11}$$

$$u = 2R_0 \sin \theta_0 - (2R_0 - \delta) \sin \theta \tag{12}$$

Using contact mechanics, the non-dimensional interference is given as (Johnson and Johnson, 1987):

$$\frac{\delta}{R_0} = \frac{2}{\pi} \frac{P}{R_0 t E} \left[\ln \left(4\pi \frac{R_0 t E}{P} \right) - 1 \right] \tag{13}$$

Where t is the thickness of the tab. This equation is solved numerically to determine the non-dimensional contact force $\frac{P}{R_0 t E}$ and the non-dimensional pullout force from Eq. (9) is given as:

$$\frac{F}{wtE} = \frac{P}{R_0 t E} \left(\frac{\sin \theta + f \cos \theta}{2 \cos \theta_0} \right) \tag{14}$$

The effect of Poisson's effects are neglected in this solution, but finite elements confirm that Poisson's ratio has little effects on the solutions.

Fig. 5a and b show the effects of the friction coefficient f , and interlocking angle θ_0 on the pullout response of the suture. High coefficients of friction f lead to relatively high strength because of increased friction at the contact point, but do not change the maximum pullout distance which is governed by geometric parameters. Higher interlocking angles θ_0 increase the strength because of increased geometrical interlocking (Fig. 5b), and also increase the maximum pullout distance because the tabs stay in contact over a longer pullout distance. The friction f and interlocking angle θ_0 have therefore positive effects on strength and energy absorption. However increasing these two parameters also increase frictional stresses, which can lead to the fracture of the tabs. The maximum tensile stress in the suture is divided into frictionless and frictional contact stresses (Malik et al., 2017), which can be evaluated from contact solutions. These frictional stresses produce the maximum tensile stresses in the solid tabs, which are plotted as function of pullout distance for different coefficient of friction (Fig. 5c) and different locking angles (Fig. 5d). The contact stresses can also be

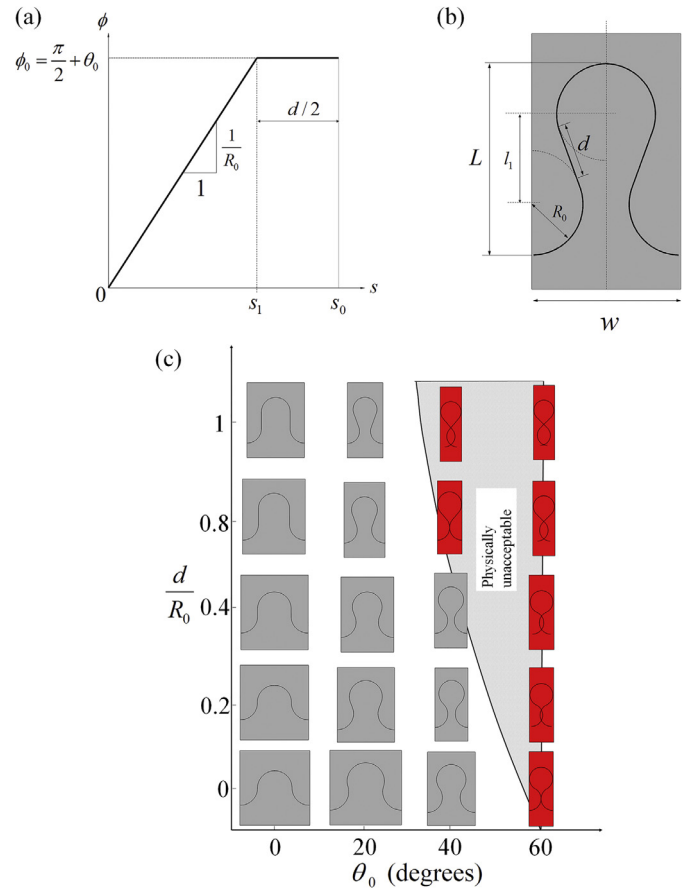


Fig. 8. (a) $(\phi-s)$ curve for a two-parameter suture; (b) Corresponding profile; (c) The “strength” of the geometrical interlocking is governed by the interlocking angle θ_0 and the plateau length d/R_0 . The geometries highlighted in red are not physically acceptable. (For interpretation of the references to color in this figure legend, the reader is referred to the web version of this article.)

illustrated with finite element results, with the lowest principal stress σ_{Emin}^{\min} (i.e. maximum pressure, Fig. 6a and b) and the highest tensile stress σ_{Emin}^{\max} (Fig. 6c). The contact pressure is distributed over the contact following the expected parabolic profile. The tensile stress is maximum at the edge of the contact surface which is “behind” the direction of sliding. Fig. 6d and e show the pullout (force-displacement) curve and the maximum local stress as func-

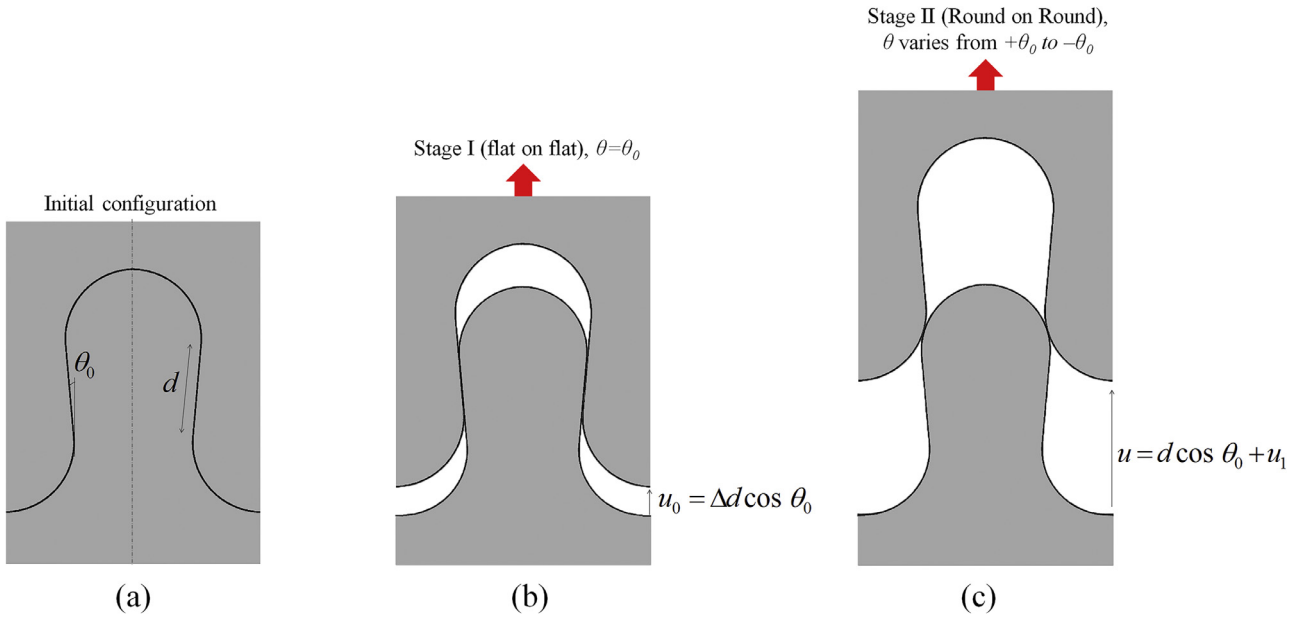


Fig. 9. Stages of the pullout for a dovetail suture; (a) Initial stage (no force applied), (b) first pullout stage where the flat faces are in contact, (c) second stage where only the rounded sections are in contact.

tion of pullout distance. The analytical solution and finite element models are in good agreement.

The interlocking angle θ_0 , and friction coefficient f , increase the maximum pulling force and total energy absorbed during pullout. However the associated local stresses in the solid may cause a premature fracture of the tab, therefore there is need for optimization. Here we performed an exhaustive search of the design space to identify the best combination(s) of design parameters for any given set of desired of normalized stiffness, strength, maximum extension, and energy absorption. The limiting factor for the design is the fracture of the solid tabs, which is governed by the strength of the material. The tabs will therefore fracture when $\sigma_{max}/E = \sigma_s/E$, where σ_{max} is the maximum tensile stress predicted from the model and σ_s is the tensile strength of the solid material. Here we present results for $\sigma_s/E = 1/100$, which is a common ratio for engineering materials (Ashby, 2011). For a given value of friction coefficient, it is therefore possible to identify the optimum locking angle that will be the largest while preventing fracture of the tabs. The strength is simply $\frac{F_{max}}{wtE}$, the maximum elongation is $\frac{u_{max}}{L}$ and the energy absorbed is given by the area under the pullout force-displacement curve,

$\frac{U}{wtLE} = \int_0^{u_{max}} \frac{F}{wtE} \frac{du}{L}$. Fig. 7a shows the allowable combinations of θ_0 and f that will prevent tab fracture and ensure the complete pullout the suture. Since strength and energy absorption both increase with θ_0 and f , the optimum combinations of θ_0 and f lie on the line defined by $\sigma_{max}/E = \sigma_s/E = 1/100$. As expected, if f is increased then θ_0 must be decreased to prevent the fracture of the tabs. Fig. 7b shows the corresponding optimal energy absorption $(\frac{U}{wtLE})_{opt}$ and the optimal strength $(\frac{F_{max}}{wtE})_{opt}$. The maximum pullout strength is achieved with a locking angle $\theta_0 = 12.75^\circ$ and a friction coefficient $f = 0$, and at a value $F_{max}/wtE \sim 0.5 \times 10^{-3}$. However, this design does not dissipate any energy upon pullout, because the frictional dissipative mechanism is absent ($f = 0$). To reach the highest energy dissipation possible f must be increased, and θ_0 must be decreased. The bell-shape of this curve shows there is an optimum point where the energy dissipation is maximum, which is achieved with a locking angle $\theta_0 = 9.25^\circ$ and friction coefficient $f = 0.06$. This exhaustive search can therefore be used to identify the suture geometry and local friction that will optimize strength and/or toughness. The results also highlight the main limitation of

this design: the maximum strength of the suture is only about 5% of the tensile strength of the solid material. In the upcoming sections we explore enriched geometries that aim at reducing the frictional contact stresses by distributing the contact over larger areas.

4.2. Dovetail-like sutures

As a first extension to the simple jigsaw geometry, we increased the contact area in order to better distribute and to decrease the contact stresses, and in particular those associated with friction. Reducing the contact stresses can delay the fracture of the solid materials, which can enable more extreme locking geometries and more efficient designs. A straight region of length d was added on the suture contour, which produced a “dovetail like” geometry (Fig. 8a,b). This dovetail suture can be described with three independent parameters: interlocking angle θ_0 , radius of curvature R_0 and length of straight segment d , which were reduced to two parameters (θ_0 and d/R_0) after normalization. Other geometrical parameters are given by:

$$\begin{cases} \phi_0 = \theta_0 + \pi/2 \\ s_0/R_0 = \phi_0 + d/2R_0 \\ w/R_0 = 4 \sin \phi_0 + 2(d/R_0) \cos \phi_0 \\ L/R_0 = 2(1 - \cos \phi_0) + (d/R_0) \sin \phi_0 \end{cases} \quad (15)$$

The $\phi(s)$ function (Fig. 8a) was defined as:

$$\begin{cases} \phi(s) = \frac{s}{R_0}, & 0 \leq s \leq s_0 - d/2 \\ \phi(s) = \phi_0, & s_0 - d/2 \leq s \leq s_0 \end{cases} \quad (16)$$

Fig. 8c shows a set of dovetail suture profiles obtained for different combinations of θ_0 and d/R_0 . For $d/R_0 = 0$ the single jigsaw geometry is recovered. With $d/R_0 > 0$ a wide range of geometries can be obtained, but some combinations of parameters lead to the contour intersecting itself. The condition for the contours not to intersect is $2R_0 < w$, which can be written:

$$\theta_0 < \arccos\left(\frac{R_0}{\sqrt{d^2 + 4R_0^2}}\right) - \arctan\left(\frac{d}{2R_0}\right) \quad (17)$$

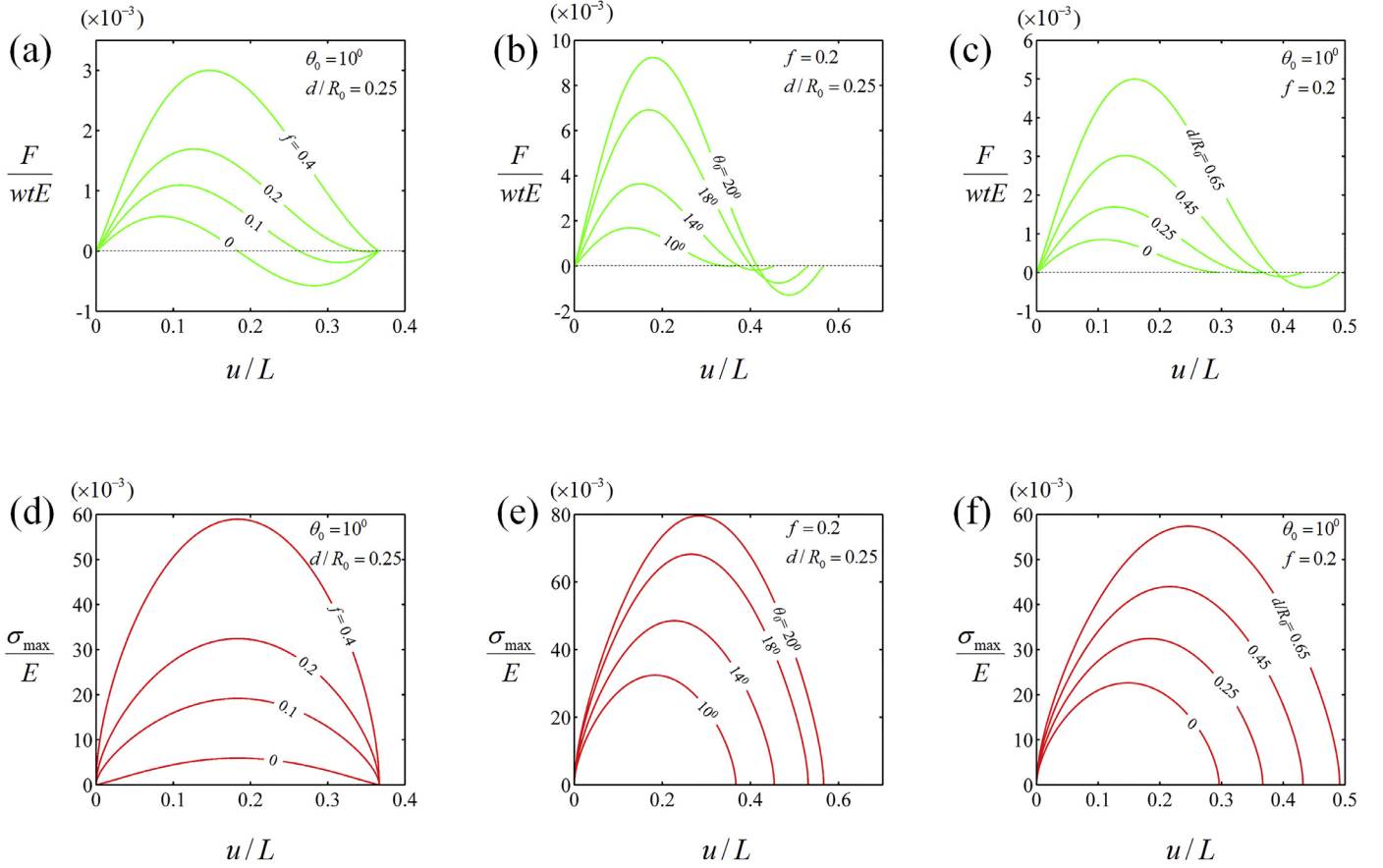


Fig. 10. Effects of (a) friction f (b) interlocking angle θ_0 , and (c) plateau length d/R_0 , on the pullout response of the suture; effects of (d) friction f (e) interlocking angle θ_0 , and (f) plateau length d/R_0 , on maximum tensile stress in the solid tabs.

On Fig. 8c, Eq. (17) defines the boundary between admissible geometries and inadmissible geometries. As the plateau length d/R_0 , increases from zero (single locking) to higher values, the range of allowable locking angles θ_0 becomes narrower. To predict the pullout response of the dovetail suture we used the same procedure as for the single jigsaw model. An analytical solution was first developed by using a 2D flat punch with rounded edge as base solution for the contact interaction (Ciavarella et al., 1998, 2002; Giannakopoulos and Chenut, 2000; Sackfield et al., 2005). The kinematics of two disks in contact is the same as that described above using Eq. (11), and the normalized contact radius a/R_0 can be determined from non-Hertzian contact solution for two similar disks in contact Eq. (18) (Johnson and Johnson, 1987).

$$\frac{\delta}{R_0} = \frac{1}{2} \left(\frac{a}{R_0} \right)^2 \left[\ln \left(16 \left(\frac{R_0}{a} \right)^2 \right) - 1 \right] \quad (18)$$

The normalized contact surface a/R_0 can be obtained by solving Eq. (18) numerically. From a/R_0 one can compute the normal force for a flat punch with rounded ends for plane stress condition is given as (Ciavarella et al., 2002):

$$\frac{P}{R_0 t E} = \frac{1}{2} \left(\frac{b}{R_0} \right)^2 \left[\frac{\pi}{2} - \frac{d}{2b} \sqrt{1 - \left(\frac{d}{2b} \right)^2} - \arcsin \left(\frac{d}{2b} \right) \right] \quad (19)$$

$$\frac{b}{R_0} = \frac{d}{2R_0} + \frac{a}{R_0} \quad (20)$$

The pullout is divided into two stages as shown in Fig. 9. The first stage involves the sliding of the flat portion and the interlocking angle remains unchanged while the contact length reduces

from d to zero. The pullout distance in the first stage is given as:

$$u_0 = \Delta d \cos \theta_0 \quad (21)$$

Where Δd is the difference in the sliding length as the pullout progresses from zero to d . At the second stage the pullout distance is the same as that of a single jigsaw which is given as:

$$u_1 = 2R_0 \sin \theta_0 - (2R_0 - \delta) \sin \theta \quad (22)$$

where δ is the interference between two disks pressed against each other and θ is used to track the evolution of the interlocking angle.

Resolving the force components vertically and normalizing by the suture width provides the average pullout force:

$$\frac{F}{wtE} = \frac{P}{R_0 t E} \left(\frac{\sin \theta + f \cos \theta}{2 \cos \theta_0 - d \sin \theta_0} \right) \quad (23)$$

The angle θ is used to track the progressive pullout of the suture, and it remains constant along the flat portion of the suture, but later evolves from $+\theta_0$ to $-\theta_0$ at the rounded ends of the suture. Fig. 10a–c show the effect of friction coefficient f , interlocking angle θ_0 , and plateau length d/R_0 , on the average pullout force. Friction (Fig. 10a) and interlocking angle (Fig. 10b) have the same effect as we observed for the single jigsaw design- they both increase maximum pullout force and energy absorption. Increasing the length d of the plateau increases the area of contact, which increases the pullout force (Fig. 10c).

The maximum tensile stress in the suture is divided into frictional contact stress and frictionless (hole in an infinite plate loaded by a frictionless pin in the in-plane direction) maximum tensile stress. The frictionless maximum stress is given as

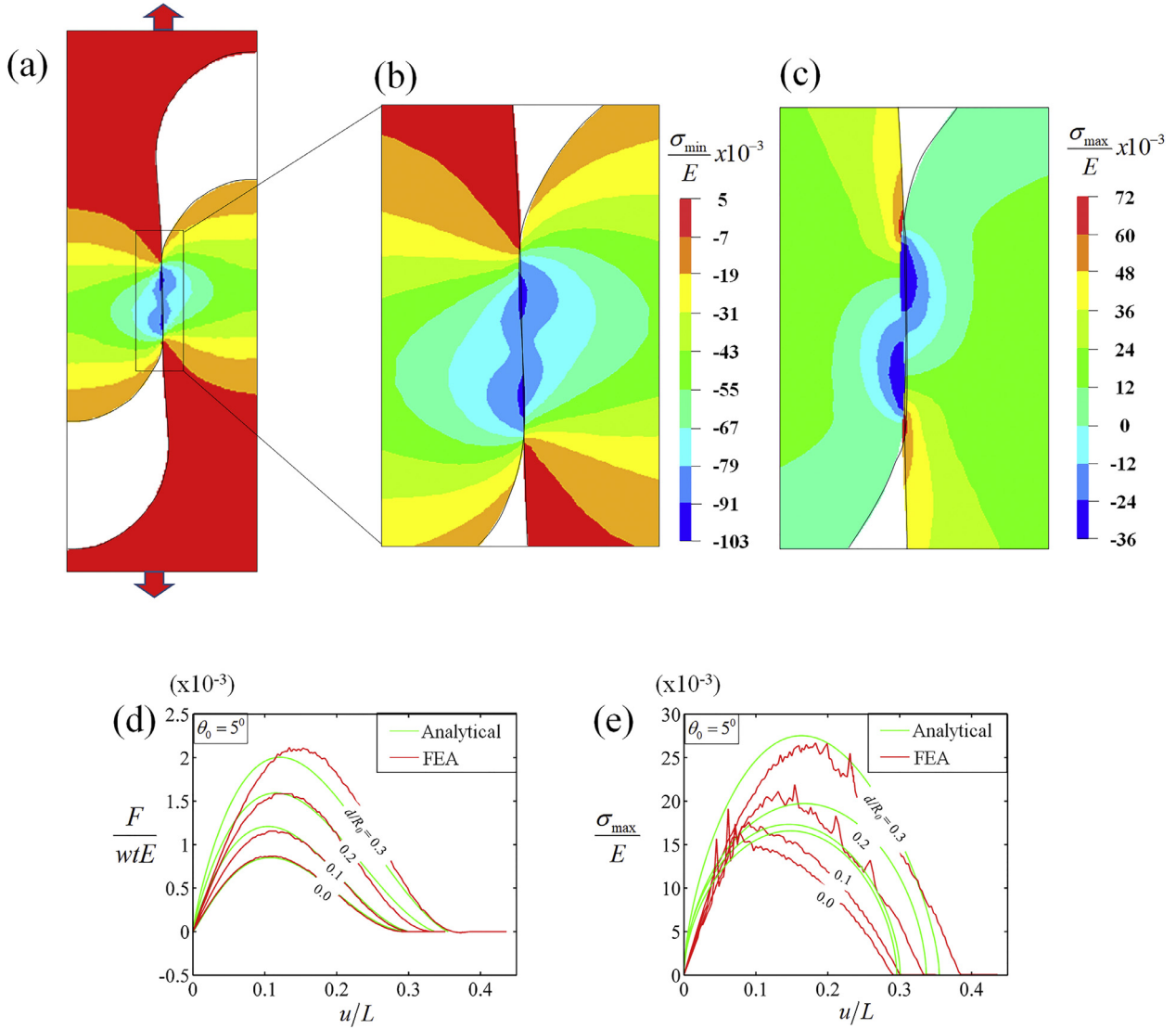


Fig. 11. (a) and (b): contour plots of maximum pressure for $\theta_0 = 5^\circ$, $d = 0.8$, and $f = 0.4$; (c) contour plot of maximum principal stress (d) and (e) traction and stresses as function of pullout distance showing a good agreement between the analytical and finite elements results.

(Ciavarella and Decuzzi, 2001):

$$\sigma_{\max}^{(P)} = \frac{P}{R_0 t} \frac{5 - \nu}{2\pi} \quad (24)$$

The sliding frictional contact stress is given as (Ciavarella et al., 2002):

$$\sigma_{\max}^{(fP)} = 2fpk \quad (25)$$

Where p is the contact pressure given as $p = \frac{2P}{\pi tb}$ and k is a geometrical factor that defines the effect of contact length ratio, $d/2b$ on the pressure distribution of flat punch with rounded edges. If $d = 0$, then $k = 1$ which reduces to a cylinder-on-cylinder contact (Ciavarella et al., 2002).

$$p = \frac{2P}{\pi tb}$$

$$k = \sqrt{\frac{1 - (2/\pi) \arcsin(d/2b)}{1 - (2/\pi) \arcsin(d/2b) - (2/\pi)(d/2b)\sqrt{1 - (d/2b)^2}}$$

$$\sigma_{\max}^{(fP)} = \frac{4Pf}{\pi tb} k \quad (26)$$

Superposition of these two solutions gives the total stress at the trailing edge of the contact:

$$\sigma_{\max} = \sigma_{\max}^{(P)} + \sigma_{\max}^{(fP)} = \frac{P}{R_0 t} \frac{5 - \nu}{2\pi} + \frac{4Pf}{\pi tb} k \quad (27)$$

Normalizing this equation gives:

$$\frac{\sigma_{\max}}{E} = \frac{1}{2\pi} \frac{P}{R_0 t E} \left[(5 - \nu) + 8 \left(\frac{R_0}{b} \right) k f \right] \quad (28)$$

The maximum stress increases with interlocking angle, plateau length, and friction (Fig. 10d, e, f). Fig. 11 shows the minimum principal stress, maximum stress contour plots and the comparison between the pullout response and maximum stress. The result shows that both the analytical and finite element models are in good agreement. For the rest of this section we used the analytical model because of its simplicity.

To identify optimum sets of design parameters, we followed the same procedure as for the single jigsaw, by performing an exhaustive parametric study on f , θ_0 and d/R_0 . In particular, we identified optimum sets of parameters that prevent fracture of the tabs, using $\sigma_s/E = 1/100$ for the tensile strength of the solid material. Fig. 12(a) shows different combinations of f and θ_0 that achieve this condition, and for four different values of d/R_0 . As expected, increasing

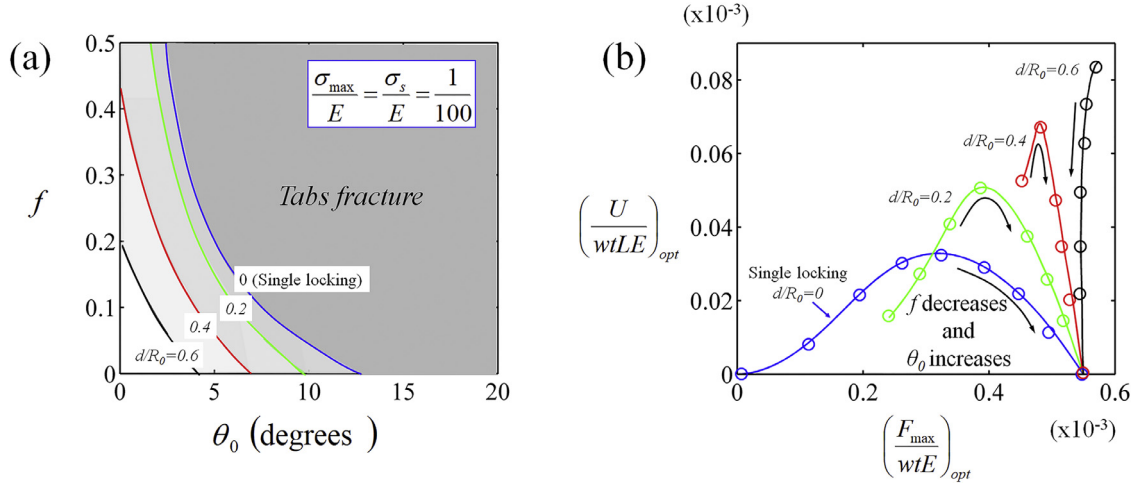


Fig. 12. (a) Possible combination of the parameters θ_0 , f , and d/R_0 for optimum designs; (b) material property map showing the optimum energy absorbed and the optimum pullout strength for different d/R_0 and for a design constraint $\sigma_s/E=1/100$.

the plateau d/R_0 must be accompanied by a reduction of f and/or θ_0 to prevent the fracture of the tab. Fig. 12b shows the corresponding optimum energy absorption and strength. Compared to the single jigsaw tab design adding straight regions produced narrower bell-shape curves, because as mentioned above the range of permissible f and θ_0 is more restricted. The dovetail design however produced higher increases energy absorption, up to 2.5 times higher than what can be obtained from the single jigsaw design. The maximum pullout strength possible is however the same, at $F_{\max}/wtE \sim 0.5 \times 10^{-3}$ for all designs. Interestingly, the optimum design achieves the highest possible strength and energy absorption simultaneously. This optimum design has a friction coefficient of 0.12, a long dovetail $d/R_0=0.6$ and a vanishingly small locking angle ($\theta_0=0.125^\circ$). A further increase in the plateau length ($d/R_0 > 0.6$) did not generate any further improvements.

4.3. Double locking sutures

The dovetail design demonstrated how distributing the contact stresses over a larger area could delay fracture of the tabs and lead to higher performance. We now examine another approach, where the pullout force is transferred over more than one contact area. "Double locking" suture geometries were obtained by enriching the $\phi(s)$ with a second segment with a nonzero slope (Fig. 13a). The most interesting cases are produced when this second slope is negative, which then produces a second locking site of radius R_1 (Fig. 13b). The slope of that segment is therefore $-1/R_1$ on the $\phi(s)$. This enriched design has therefore three independent non-dimensional geometrical parameters: (i) interlocking angle θ_0 , (ii) radii ratio R_0/R_1 , (iii) cumulative angular function ϕ_0/ϕ_1 . The suture angle function is written:

$$\begin{cases} \phi(s) = \frac{s}{R_0}, & 0 \leq s \leq s_1 \\ \phi(s) = 2\phi_0 - \frac{s}{R_1}, & s_1 \leq s \leq s_0 \end{cases} \quad (29)$$

Other geometrical parameters are written:

$$\begin{cases} \phi_0 = \theta_0 + \pi/2 \\ \phi_1 = -\theta_1 + \pi/2 \\ s_1 = R_0\phi_0 \\ s_0 = R_0\phi_0 + R_1(\theta_0 + \theta_1) \\ w = 2[2(R_0 + R_1)\sin\phi_0 - 2R_1\sin\phi_1] \\ L = 2[R_0(1 - \cos\phi_0) - R_1(\cos\phi_0 - \cos\phi_1)] \end{cases} \quad (30)$$

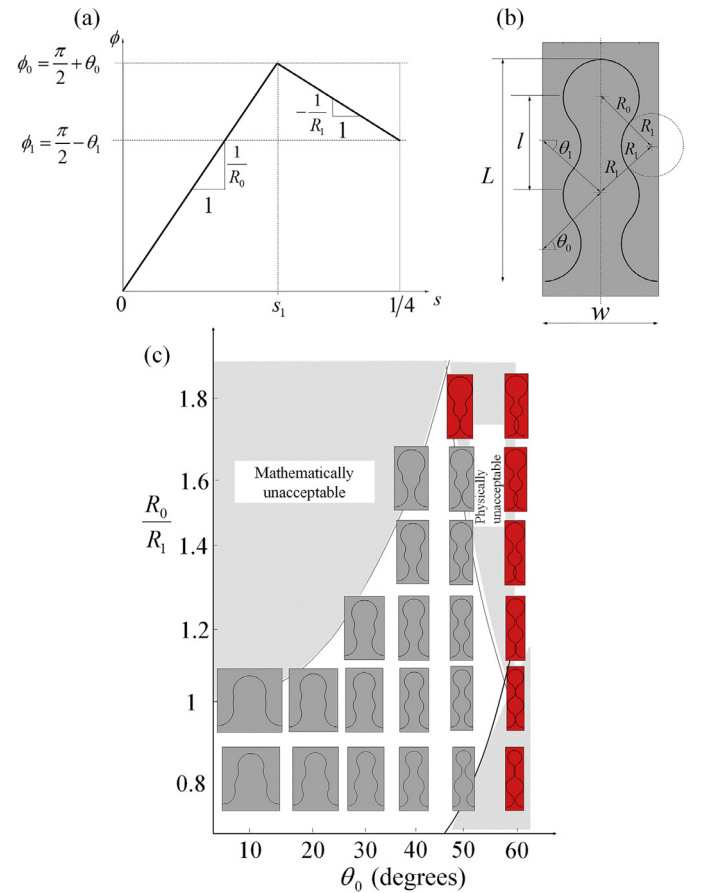


Fig. 13. (a) ϕ - s curve for a two-parameter suture; (b) Corresponding profile; (c) The "strength" of the geometrical interlocking is governed by the interlocking angle θ_0 and by R_0/R_1 . The geometries highlighted in red are not physically acceptable. (For interpretation of the references to color in this figure legend, the reader is referred to the web version of this article.)

There are geometric constraints on R_0/R_1 and θ_0 which restrict the range of possible designs for this suture. The transition angle θ_1 can be written:

$$\theta_1 = \arccos\left(\frac{1}{2}\left(\frac{R_0}{R_1} + 1\right)\cos\theta_0\right) \quad (31)$$

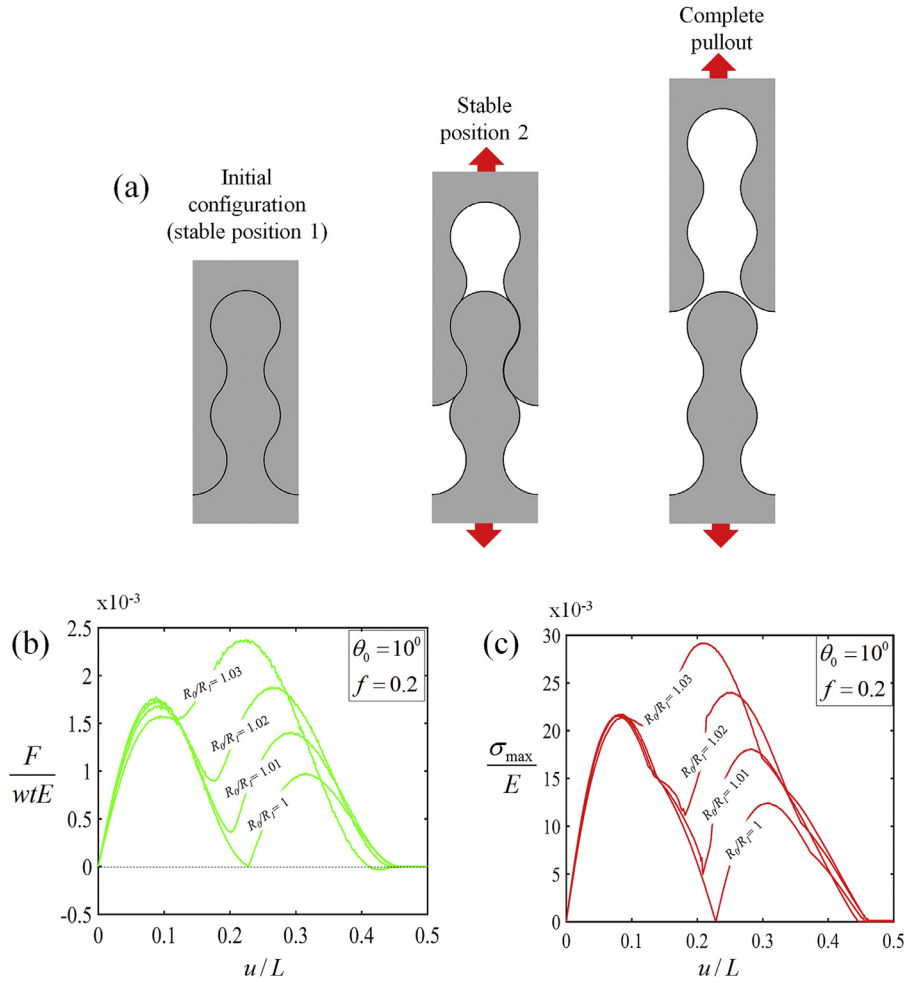


Fig. 14. (a) Progressive pullout showing the two locking stages; effects of radii ratio R_0/R_1 on (b) pullout response and (c) maximum tensile stress in the solid tabs.

However Eq. (31) has a solution only if:

$$\frac{R_0}{R_1} \leq \frac{2}{\cos \theta_0} - 1 \quad (32)$$

In addition the contour of the suture cannot intersect, therefore a physical condition is given as:

$$\frac{1 - \cos \theta_0}{\cos \theta_0} < \frac{R_0}{R_1} < \frac{\cos \theta_0}{1 - \cos \theta_0} \quad (33)$$

Eqs. (32) and (33) define the boundaries of admissible geometries for this type of sutures (Fig. 13c). The pullout response can be decomposed into two stages. In the first stage, the two pairs of locking sites are in contact (Fig. 14a). As the pullout progresses the system may reach a second stable locking configuration, which can occur if $R_0/R_1 \geq 1$. Further pullout from that position only involves one contact pair. Using Fig. 3a–c, and 13b above, we can derive the kinematics relations for stage 1:

$$\frac{\delta}{R_0} = \left(1 + \frac{R_1}{R_0}\right) \left[1 - \frac{\cos \theta_0}{\cos \theta}\right] \quad (34)$$

$$\frac{u}{L} = \frac{\sin \theta_0 - \sin \theta + 0.5(\delta/R_0) \sin \theta}{1 + 3 \sin \theta_0} \quad (35)$$

$$\frac{F}{wtE} = \frac{P}{R_0 t E} \left(\frac{\sin \theta + f \cos \theta}{\cos \theta_0}\right) \quad (36)$$

At the second stage:
$$\frac{u}{L} = \frac{3 \sin \theta_0 - \sin \theta + 0.5(\delta/R_0) \sin \theta}{1 + 3 \sin \theta_0}$$

$$(37)$$

$$\frac{F}{wtE} = \frac{P}{R_0 t E} \left(\frac{\sin \theta + f \cos \theta}{2 \cos \theta_0}\right) \quad (38)$$

These equations are combined to compute the pullout response of the suture. We found that f and θ_0 have the expected effect: they both increase the strength and energy absorption of the suture, but they also increase the maximum stress in the tabs. Fig. 14b shows the effect of R_0/R_1 on the pullout response. The case $R_0/R_1 = 1$ produces two force peaks, the first peak corresponding to the force generated by two contact pairs, the second peak being generated by only one contact pair. As a result, the second peak is half of the first one. Interestingly increasing R_0/R_1 increases the second peak, because the second pullout stage is generated by a larger geometric interference between the tabs. This effect is very sensitive to the value of R_0/R_1 . For $R_0/R_1 = 1.02$ the two peaks are equal, and for $R_0/R_1 = 1.03$ the second peak becomes higher than the first. This “geometric hardening” can generate some attractive mechanisms at large length scales (Mirkhalaf and Barthelat, 2017).

The maximum tensile stresses can be divided into a contribution from normal forces, and a contribution from the frictional forces.

- (i) Hole in an infinite plate loaded by a frictionless pin in the in-plane direction (Ciavarella and Decuzzi, 2001; Persson, 1964): in this configuration the inner side of a hole is loaded by a contact force acting along the radial direction. The resulting

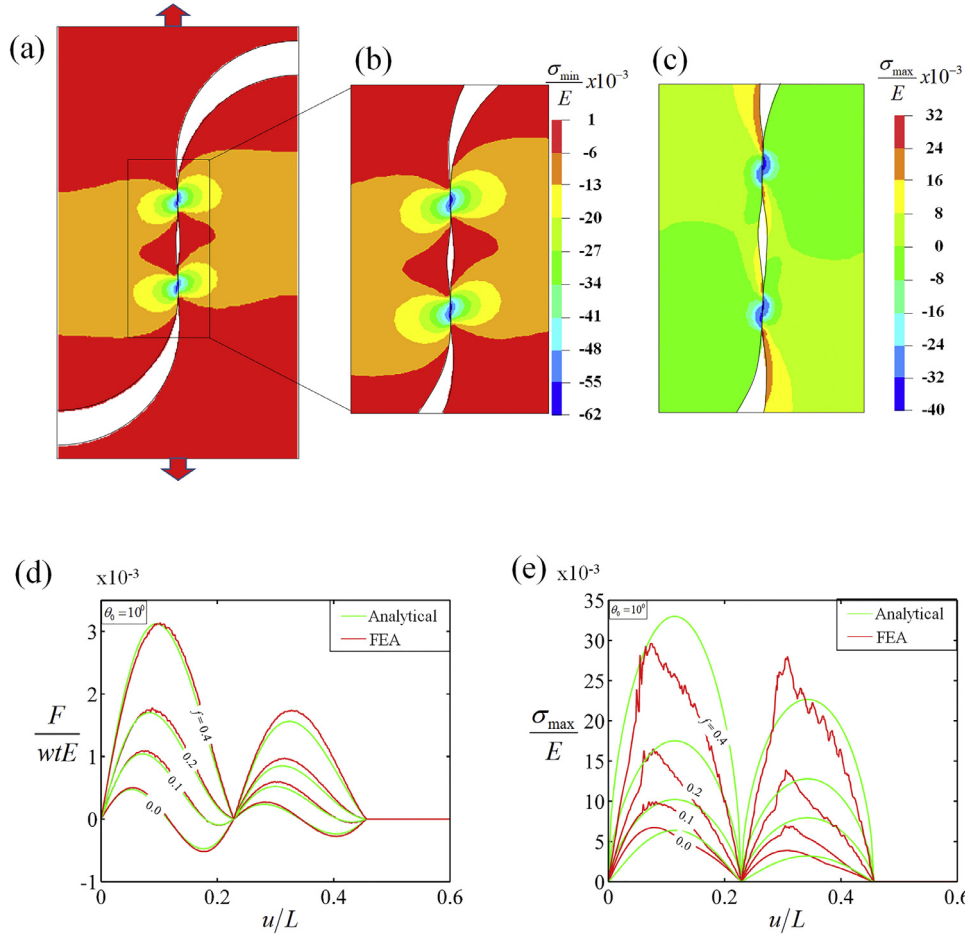


Fig. 15. (a) and (b) contour plots of maximum pressure for $\theta_0 = 10^\circ$ and $f = 0.4$; (c) contour plot of maximum principal stress (d) and (e) traction and stresses as function of pullout distance showing a good agreement between the analytical and finite elements results.

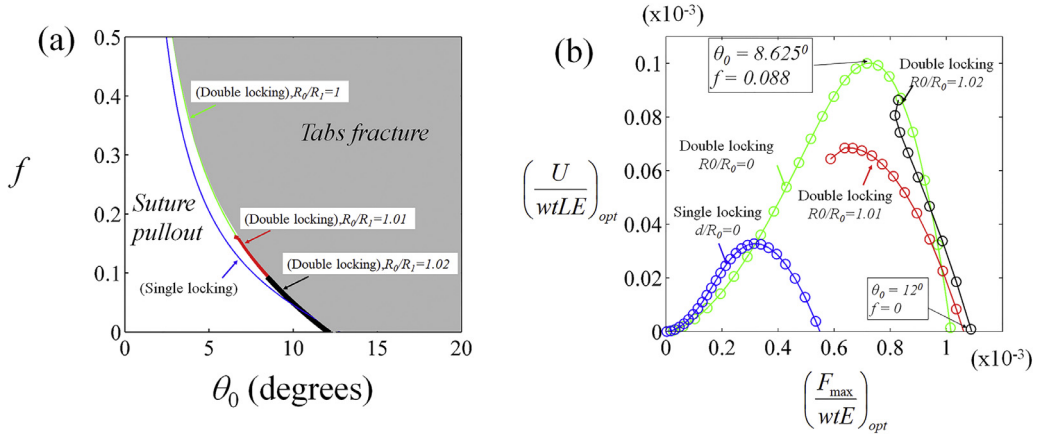


Fig. 16. (a) Possible combination of the parameters θ_0 , f and R_0/R_1 for optimum designs; (b) material property map showing the optimum energy absorbed and the optimum pullout strength, for $R_0/R_1 = 1, 1.01, 1.02$ and with the design constraint $\sigma_s/E = 1/100$.

maximum tensile stress is the tangential stress at the edge of the contact area.

$$\sigma_{max}^{(P)} = \frac{P}{Rt} \frac{5 - \nu}{2\pi} \quad (39)$$

- (ii) *Periodic frictional contact:* With a sliding frictional contact, the maximum tensile stress is close to the trailing edge of contact. A solution was derived using Kolosov-Muskhelishvili general formula and the theory of automorphic functions (Dundurs et al., 1973; Goryacheva and Martynyak, 2014;

Kuznetsov, 1976). A sinusoidal periodic contact problem is considered and the sinusoidal equation with amplitude Δ and wavelength l is given as:

$$y = \delta - \Delta \left(1 - \cos \frac{2\pi x}{l} \right) \quad (40)$$

Where x is the coordinate of the interface, δ is the interference between two contacting tabs. Assume that the contact area and the amplitude is small ($a < R$ and $\Delta < R$), the maximum pressure is

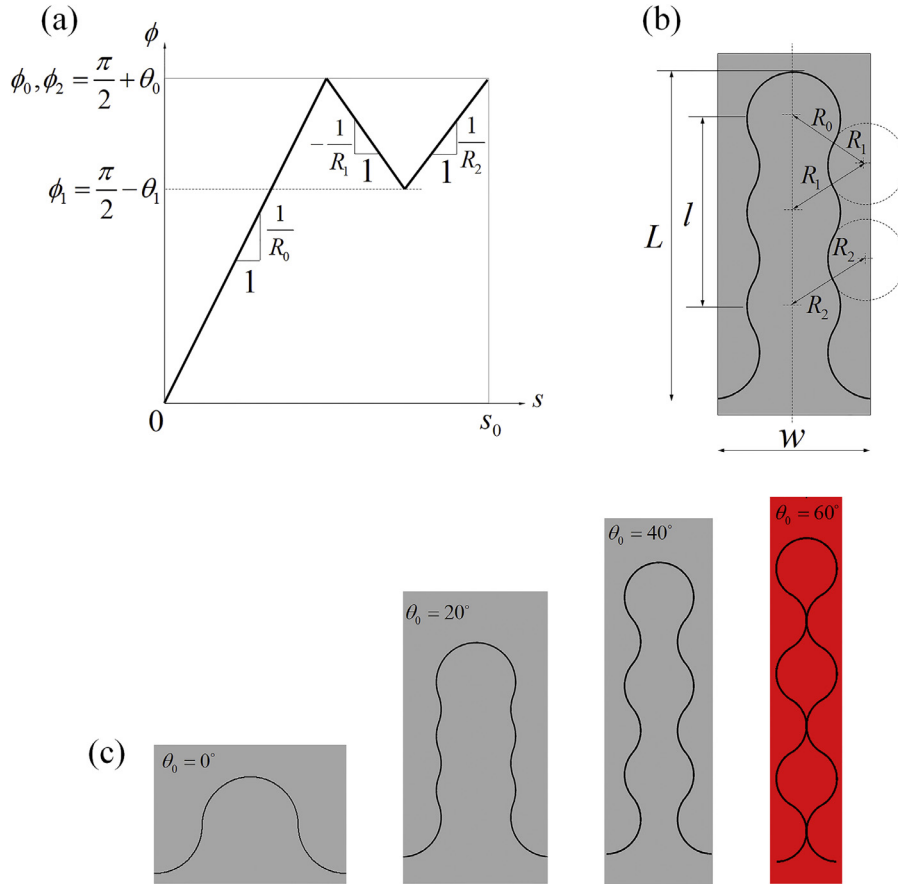


Fig. 17. (a) $(\phi-s)$ curve for a two-parameter suture; (b) Corresponding profile; (c) Here the “strength” of the geometrical interlocking is governed by the interlocking angle θ_0 and by the number of locking sites. The cases highlighted in red is not physically acceptable. (For interpretation of the references to color in this figure legend, the reader is referred to the web version of this article.)

given as:

$$p_0 = \frac{El}{2\pi R_0} \sin\left(\frac{\pi b}{l}\right) \quad (41)$$

Where R_0 is the radius of curvature, b is the half-width of contact area and it is given as $b = \frac{l}{\pi} \arcsin\left(\frac{\pi a}{l}\right)$, E , ν are the elastic modulus and Poisson’s ratio for the solid material. The maximum tangential stress in frictional contact is given as $\sigma_{\max}^{(fp)} = 2fp_0$ (Johnson and Johnson, 1987), and the superposition of both frictionless and periodic frictional contact stresses gives the maximum tensile stress in the suture. Fig. 14c shows the dependence of maximum tensile stress on radii ratio R_0/R_1 . The maximum pressure and maximum stress from the finite element model are shown in Fig. 15a–c below. The maximum stress occurred at the edge of the contact region (Fig. 15c) which agrees with the analytical solution. Fig. 15d and e shows excellent agreement between the finite elements and analytical predictions in terms of pullout response and maximum tensile stress within the material.

A design optimization was performed on the geometry of the double locking design, with the maximum stress in the tab as design constraint. The material fractures when $\frac{\sigma_{\max}}{E} = \frac{\sigma_S}{E}$ and Fig. 16a shows for any given radii ratio R_0/R_1 , the possible combination(s) of friction coefficient f and interlocking angle θ_0 from the optimization method by setting the strength-modulus ratio to $\frac{\sigma_S}{E} = \frac{1}{100}$. The results show that R_0/R_1 has little effect on the failure map within the range explored. Fig. 16b shows the optimum energy absorption and strength of material distribution for different designs. Compared to the single locking design, the double locking design increases the optimum strength by a factor of two, and the opti-

imum energy absorption by a factor of about three. When R_0/R_1 is increased the possible range of angles and friction becomes narrower, and relatively high values of R_0/R_1 ($R_0/R_1 = 1.02$) become sub-optimal in terms of energy absorption. For all designs, the optimum material properties are achieved with a low friction coefficient f , and relatively high interlocking angle θ_0 .

4.4. Multi-locking ($N > 2$) suture geometries

With the same objective to decrease the frictional stress by creating more contact points, we finally explore locking geometries with N ($N > 2$) pairs of locking sites. Fig. 17a shows a $\phi(s)$ function for a $N=3$ design. There are seven independent, normalized geometric parameters for $N=3$: θ_0 , R_0/R_1 , R_0/R_2 , R_1/R_2 , ϕ_0/ϕ_1 , ϕ_0/ϕ_2 , and ϕ_1/ϕ_2 . More generally, multi-locking sutures with N contact pairs have $1 + 2 \sum_{k=1}^{N-1} (N-k)$ independent, normalized geometric parameters: θ_0 , R_0/R_1 , ..., R_0/R_{N-1} , ϕ_0/ϕ_1 , ..., ϕ_0/ϕ_{N-1} . The previous section showed that in terms of strength and energy absorption $R_0/R_1 = 1$ is the best design for double locking sutures. Therefore in this section we only consider cases where $R_0 = R_1 = \dots = R_{N-1} = 1$.

A closed form for the pullout response can be obtained by extending the $N=2$ solution. There are N stages of pullout, and the pullout force for the first stage is given as:

$$\frac{F}{wtE} = \frac{NP}{R_0 t E} \left(\frac{\sin \theta + f \cos \theta}{2 \cos \theta_0} \right) \quad (42)$$

The equations for stress are similar to the double locking and the major difference is the half-width of contact b and length l , which is given as $b = \frac{l}{\pi} \arcsin\left(\frac{\pi a}{l}\right)$, for all sutures with $N > 1$.

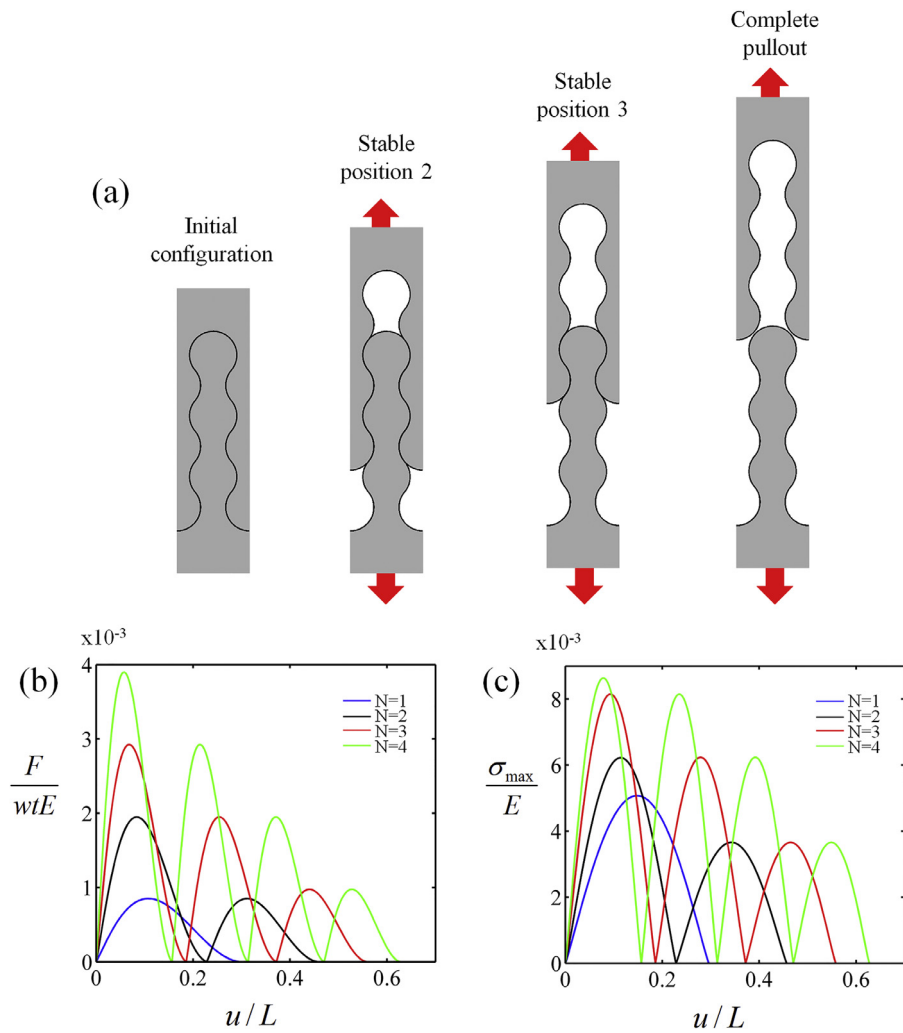


Fig. 18. (a) Progressive pullout showing the three locking stages for suture with $N=3$; effect of number of locking on (b) average pullout force of the suture, and (c) maximum tensile stress in the solid tabs.

Fig. 18b and c show the effect of N on the pullout force and maximum tensile stress. For each design there is a total of N local peaks of force corresponding to N stages of pullout. The first peak is the maximum pullout force, and it increases proportionally with N because of the addition of locking sites of equal strength. The peaks then decrease linearly until complete pullout. For comparison we also performed finite element simulations, with some representative results shown in Fig. 19. The progressive pullout was captured in the models (Fig. 19a) and we obtained good agreement with the closed form solution in terms of pullout behaviour (Fig. 19b) and maximum stress (Fig. 19c).

The failure transition map (Fig. 20a) is not affected by a significant by N . The material property map for $N=1$ to $N=7$ (Fig. 20b) reveal that the optimum strength increases up to $N=4-5$, but then decreases thereafter. The optimum energy absorption increases by a significant margin up to $N=4-5$, after which the gain is marginal for $N=6$ and 7, and above $N=7$, the optimum energy absorption continuously decreases.

5. Summary

Sutured interfaces and geometric interlocking are common in natural materials. In this study we used a morphometric method to capture the contour of sutures by using the cumulative angular function $\phi(s)$ as a function of curvilinear position s . The two di-

mensional profile (x - y) of the suture is then easily reconstructed from $\phi(s)$. While the method is simple, relatively complex profiles can be captured using only a few geometrical parameters. Importantly, the method allows for re-entrant features, an essential characteristic of interlocking sutures. The study starts with a simple jigsaw-like model which is enriched with additional features (plateau regions in dovetail-like sutures, multiple locking sites). For each case, closed form solutions are developed to capture the full nonlinear pullout response and to predict the maximum stress (and potential fracture) in the solid material. These closed form solutions are in close agreement with finite elements. A “brute force” optimization approach was used on each type of design, where every combination of geometrical parameters is examined. We could then identify the optimum parameters for pullout strength and/or energy absorption. Fig. 21 summarizes our finding by showing the best design and their performance. The single locking material is largely outclassed by all the other designs, and we found that the best geometry is the multi-locking tab with $N=5$ (using a limit strength for the solid of $\frac{\sigma_s}{E} = \frac{1}{100}$, which is typical of engineering materials). For comparison, the pullout of a perfectly straight cylindrical rod or fiber would require an initial compressive stress across the interface to generate any pullout force. In fiber reinforced ceramic-ceramic composites, this initial compression can be generated, for example, by thermal expansion mismatch between fiber and matrix (Evans, 1990). In contrast, our sutures start in a

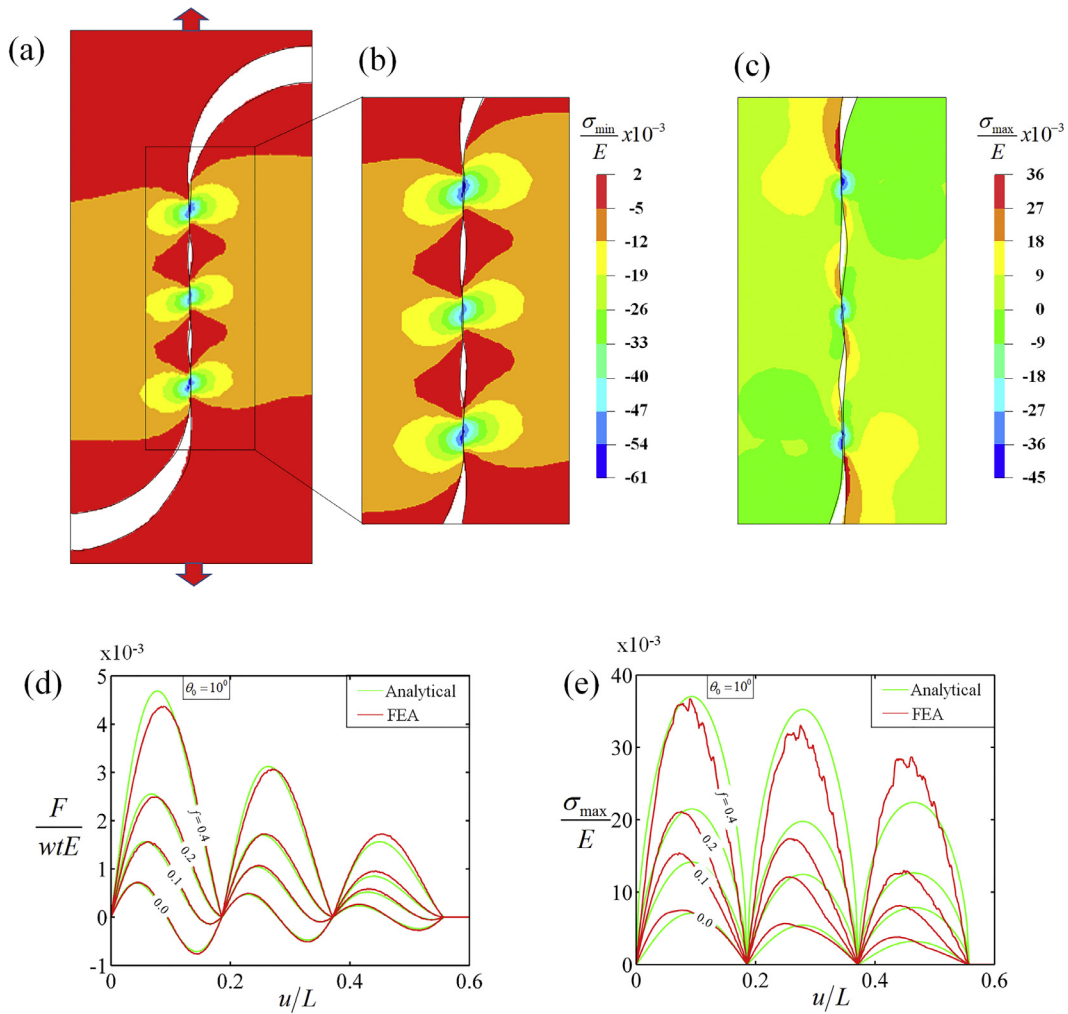


Fig. 19. (a) and (b) contour plots of maximum pressure for $\theta_0 = 10^\circ$, $N = 3$, and $f = 0.4$; (c) contour plot of maximum principal stress (d) and (e) traction and stresses as function of pullout distance showing a good agreement between the analytical and finite elements results.

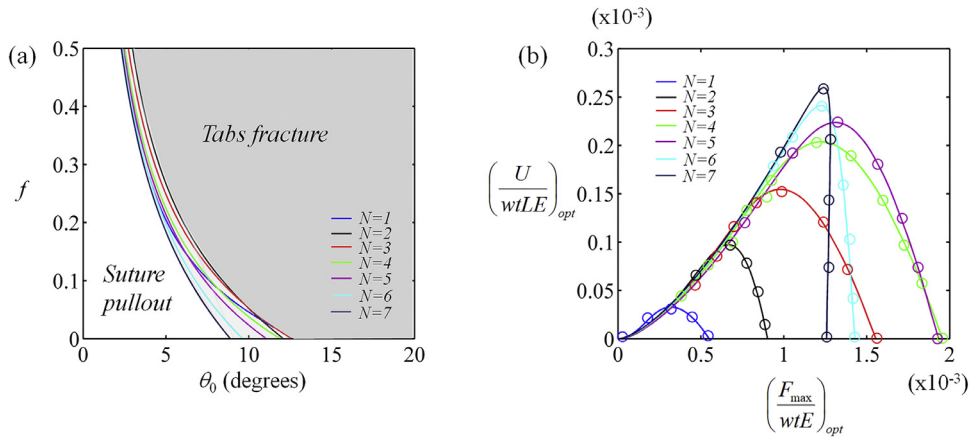


Fig. 20. (a) Possible combinations of the parameters θ_0 , f and N for optimum designs; (b) Material property map showing the optimum energy absorbed and the optimum pullout strength, for design constraints $\sigma_s/E = 1/100$.

stress-free state, and compression across the interfaces is generated by geometric interference as the suture is pullout out. Overall the limiting factor for optimization is the frictional stress, and the results show that it is very advantageous to add more contact points to decrease that stress. For the same reason it is also preferable to use very low coefficients of frictions. This result raises an

interesting hypothesis on the function of the protein layer in natural sutured lines. These soft proteins are often described as essential to provide compliance and toughness at the interface. Our result suggests that their function could also be to “lubricate” the suture line to prevent the fracture of the solid structures. These models can serve as guidelines to design and optimization of non-

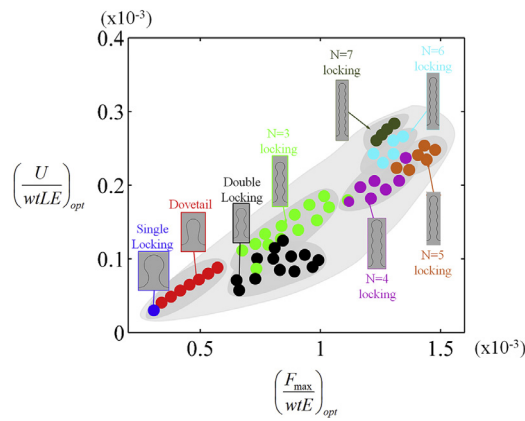


Fig. 21. Material property map showing the optimum energy absorbed and the optimum pullout strength for all the designed explored in this study ($\sigma_s/E=1/100$).

adhesive sutures with arbitrary shapes from multilinear signatures or sutures made of arc of circles and lines.

Acknowledgements

This work was supported by a Discovery Grant from the Natural Sciences and Engineering Research Council of Canada (NSERC). IAM was supported by a Scholarship from the Nigerian Government through the National Universities commission.

References

- Achrai, B., Bar-On, B., Wagner, H.D., 2014. Bending mechanics of the red-eared slider turtle carapace. *J. Mech. Behav. Biomed. Mater.* 30, 223–233.
- Allen, E.G., 2007. Understanding ammonoid sutures: New insight into the dynamic evolution of Paleozoic suture morphology. In: Landman, N.H., Davis, R.A., Mapes, R.H. (Eds.), *Cephalopods Present and Past: New Insights and Fresh Perspectives*, pp. 159–180.
- Ashby, M.F., 2011. Chapter 4—material property charts. In: *Materials Selection in Mechanical Design*. Butterworth-Heinemann, Oxford, pp. 57–96.
- Barthelat, F., et al., 2007. On the mechanics of mother-of-pearl: a key feature in the material hierarchical structure. *J. Mech. Phys. Solids* 55 (2), 306–337.
- Barthelat, F., Yin, Z., Buehler, M.J., 2016. Structure and mechanics of interfaces in biological materials. *Nat. Rev. Mater.* 1 (4).
- Chen, I.H., Yang, W., Meyers, M.A., 2015. Leatherback sea turtle shell: a tough and flexible biological design. *Acta Biomaterialia* 28, 2–12.
- Ciavarella, M., Decuzzi, P., 2001. The state of stress induced by the plane frictionless cylindrical contact. I. The case of elastic similarity. *Int. J. Solids and Struct.* 38 (26–27), 4507–4523.
- Ciavarella, M., Hills, D.A., Monno, G., 1998. The influence of rounded edges on indentation by a flat punch. *Proc. Inst. Mech. Eng., Part C* 212 (4), 319–327.
- Ciavarella, M., Macina, G., Demelio, G.P., 2002. On stress concentration on nearly flat contacts. *J. Strain Anal. Eng. Design* 37 (6), 493–501.
- Coats, B., Margulies, S.S., 2006. Material properties of human infant skull and suture at high rates. *J. Neurotrauma* 23 (8), 1222–1232.
- Cray, J., Mooney, M.P., Siegel, M.I., 2010. Timing of ectocranial suture activity in Pan troglodytes as related to cranial volume and dental eruption. *Anatom. Rec.* 293 (8), 1289–1296.
- Dundurs, J., Tsai, K.C., Keer, L.M., 1973. Contact between elastic bodies with wavy surfaces. *J. Elast.* 3 (2), 109–115.
- Dunlop, J.W.C., Weinkamer, R., Fratzl, P., 2011. Artful interfaces within biological materials. *Mater. Today* 14 (3), 70–78.
- Evans, A.G., 1990. Perspective on the development of high-toughness ceramics. *J. Am. Ceramic Soc.* 73 (2), 187–206.
- Fang, Y., et al., 2015. 3D deep shape descriptor. 2015 IEEE Conference on Computer Vision and Pattern Recognition (CVPR).
- Fratzl, P., Burgert, I., Gupta, H.S., 2004. On the role of interface polymers for the mechanics of natural polymeric composites. *Phys. Chemist. Chem. Phys.* 6 (24), 5575–5579.
- Genkal, S.I., Popovskaya, G.I., 2008. Centric diatom algae of the Selenga River and its delta branches. *Inland Water Biol.* 1 (2), 120–128.
- Giannakopoulos, Suresh, Chenu, 2000. Similarities of stress concentrations in contact at round punches and fatigue at notches: implications to fretting fatigue crack initiation. *Fatigue Fracture Eng. Mater. Struct.* 23 (7), 561–571.
- Goryacheva, I.G., Martynyak, R.M., 2014. Contact problems for textured surfaces involving frictional effects. *Proc. Inst. Mech. Eng., Part J* 228 (7), 707–716.
- Haldar, S., Sain, T., Ghosh, S., 2017. A novel high symmetry interlocking micro-architecture design for polymer composites with improved mechanical properties. *Int. J. Solids Struct.* 124 (Supplement C), 161–175.
- Johnson, K.L., Johnson, K.L., 1987. *Contact Mechanics*. Cambridge University Press.
- Kim, H.-K., Kim, J.-D., 2000. Region-based shape descriptor invariant to rotation, scale and translation. *Signal Process.* 16 (1–2), 87–93.
- Kuznetsov, E.A., 1976. Periodic contact problem for half-plane allowing for forces of friction. *Soviet Appl. Mech.* 12 (10), 1014–1019.
- Lee, N., et al., 2014. Hierarchical multiscale structure-property relationships of the red-bellied woodpecker (*Melanerpes carolinus*) beak. *J. R. Soc. Interface* 11 (96).
- Li, Y., Ortiz, C., Boyce, M.C., 2011. Stiffness and strength of suture joints in nature. *Phys. Rev. E* 84 (6).
- Li, Y., Ortiz, C., Boyce, M.C., 2012. Bioinspired, mechanical, deterministic fractal model for hierarchical suture joints. *Phys. Rev. E* 85 (3).
- Li, Y., Ortiz, C., Boyce, M.C., 2013. A generalized mechanical model for suture interfaces of arbitrary geometry. *J. Mech. Phys. Solids* 61 (4), 1144–1167.
- Lin, E., et al., 2014a. 3D printed, bio-inspired prototypes and analytical models for structured suture interfaces with geometrically-tuned deformation and failure behavior. *J. Mech. Phys. Solids* 73, 166–182.
- Lin, E., et al., 2014b. Tunability and enhancement of mechanical behavior with additively manufactured bio-inspired hierarchical suture interfaces. *J. Mater. Res.* 29 (17), 1867–1875.
- Malik, I.A., Barthelat, F., 2016. Toughening of thin ceramic plates using bioinspired surface patterns. *Int. J. Solids Struct.*
- Malik, I.A., Mirkhalaf, M., Barthelat, F., 2017. Bio-inspired “jigsaw”-like interlocking sutures: modeling, optimization, 3D printing and testing. *J. Mech. Phys. Solids* 102, 224–238.
- Maloul, A., et al., 2014. Characterization of craniofacial sutures using the finite element method. *J. Biomech.* 47(1): p. 245–252.
- Maloul, A., et al., 2014. Characterization of craniofacial sutures using the finite element method. *J. Biomech.* 47 (1), 245–252.
- Manoylov, K.M., Ognjanova-Rumenova, N., Stevenson, R.J., 2009. Morphotype variations in subfossil diatom species of Aulacoseira in 24 Michigan Lakes, USA. *Acta Botanica Croatica* 68 (2), 401–419.
- Mirkhalaf, M., Barthelat, F., 2017. Design, 3D printing and testing of architected materials with bistable interlocks. *Extreme Mech. Lett.* 11 (Supplement C), 1–7.
- Mirkhalaf, M., Dastjerdi, A.K., Barthelat, F., 2014. Overcoming the brittleness of glass through bio-inspiration and micro-architecture. *Nat. Commun.* 5, 3166.
- Miura, T., et al., 2009. Mechanism of skull suture maintenance and interdigitation. *J. Anatomy* 215 (6), 642–655.
- Persson, A., On the stress distribution of cylindrical elastic bodies in contact 1964: inst.
- Sackfield, A., Dini, D., Hills, D.A., 2005. The finite and semi-infinite tilted, flat but rounded punch. *Int. J. Solids Struct.* 42 (18), 4988–5009.
- Saunders, W.B., Work, D.M., Nikolaeva, S.V., 1999. Evolution of complexity in paleozoic ammonoid sutures. *Science* 286 (5440), 760–763.
- Zavattieri, P.D., Hector Jr., L.G., Bower, A.F., 2008. Cohesive zone simulations of crack growth along a rough interface between two elastic-plastic solids. *Eng. Fracture Mech.* 75 (15), 4309–4332.
- Zhang, W., et al., 2012. Microstructure and mechanical property of turtle shell. *Theor. Appl. Mech. Lett.* 2 (1), 014009.